## REPORT

# Extremely efficient internal exciton dissociation through edge states in layered 2D perovskites

J.-C. Blancon,[1] H. Tsai,[1,2] W. Nie,[1] C. C. Stoumpos,[3] L. Pedesseau,[4] C. Katan,[5] M. Kepenekian,[5] C. M. M. Soe,[3] K. Appavoo,[6] M. Y. Sfeir,[6] S. Tretiak,[1] P. M. Ajayan,[2] M. G. Kanatzidis,[3,7] J. Even,[4] J. J. Crochet,[1]* A. D. Mohite[1]*

Understanding and controlling charge and energy flow in state-of-the-art semiconductor quantum wells has enabled high-efficiency optoelectronic devices. Two-dimensional (2D) Ruddlesden-Popper perovskites are solution-processed quantum wells wherein the band gap can be tuned by varying the perovskite-layer thickness, which modulates the effective electron-hole confinement. We report that, counterintuitive to classical quantum-confined systems where photogenerated electrons and holes are strongly bound by Coulomb interactions or excitons, the photophysics of thin films made of Ruddlesden-Popper perovskites with a thickness exceeding two perovskite-crystal units (>1.3 nanometers) is dominated by lower-energy states associated with the local intrinsic electronic structure of the edges of the perovskite layers. These states provide a direct pathway for dissociating excitons into longer-lived free carriers that substantially improve the performance of optoelectronic devices.

Two-dimensional (2D) Ruddlesden-Popper perovskites (RPPs) are a class of quantum well (QW)–like materials described by the formula $A_nA'_{n-1}M_nY_{3n+1}$, where A and A' are cations, M is metal, and Y is halide; the value of $n$ determines the QW thickness and, as a result, the degree of quantum and dielectric confinement as well as the optical band gap (or color) (*1–9*). They have emerged as an alternative to bulk (3D) organic-inorganic (hybrid) perovskites because of their technologically relevant photostability and chemical stability coupled with high-performance optoelectronic devices (*10–12*). Compared with 3D perovskites and classical semiconductor-based QWs, RPPs offer tremendous advantages because of the tunability of their optoelectronic properties through both chemical and quantum-mechanical degrees of freedom. For two decades, RPP crystals with $n = 1$ (*5, 6, 13–15*) have been studied the most with few prototypes of

optoelectronic devices (*3, 16*). Recently, the synthesis of phase-pure (purified to one $n$ value) 2D perovskites with high $n$ values ($n = 2$ to 5) was achieved (*4*), which led to the demonstration of high-efficiency thin-film solar cells based on RPPs of $n = 3$ and 4 with technology-relevant stability (*12*). However, there is limited understanding of the fundamental physical properties of phase-pure 2D perovskites of high $n$ value in thin films typically used for optoelectronic applications. Furthermore, the fate of photogenerated electron-hole pairs and the underlying photophysical processes such as charge separation and recombination are unknown.

We investigated photophysical and optoelectronic properties of phase-pure homogenous 2D perovskites and show that in thin films (fig. S1) for $n > 2$, there exists an intrinsic mechanism for dissociation of the strongly bound electron-hole pairs (excitons) to long-lived free carriers provided by lower-energy states at the edges of the layered perovskites. Moreover, once carriers are trapped in these edge states, they remain protected and do not lose their energy through nonradiative processes and can contribute to photocurrent in a photovoltaic (PV) device or radiatively recombine efficiently as desired for light-emission applications. We validate these findings through PV devices with record efficiencies and two-orders-higher photoluminescence quantum yields (PLQY) using $n > 2$ layered perovskites.

The crystal structure and evidence for phase purity of the investigated layered 2D perovskite family of $(BA)_2(MA)_{n-1}Pb_nI_{3n+1}$ with $n = 1$ to 5 are shown in Fig. 1, A and B. In order to under-

stand the origin of the thin-film optical properties, we compared them to those of their exfoliated crystal counterparts prepared by mechanically exfoliating few layers of pristine RPP crystals. The optical absorption and photoluminescence (PL) properties of the thin films and exfoliated crystals are illustrated in Fig. 1, C to F (fig. S1) (*17*), along with bulk $CH_3NH_3PbI_3$ perovskites for comparison.

There was a marked difference in the optical properties of the thin films and exfoliated crystals (Fig. 1, C to H; table S1; and fig. S2) (*17*). In the exfoliated crystals, band-gap absorption and emission increased monotonously from 1.85 to 2.42 eV with decreasing $n$ from 5 to 1 (QW thickness varying from 3.139 to 0.641 nm), which is expected from quantum and dielectric confinement resulting in many-body interactions and large exciton binding energies at room temperature (*5–9, 13, 18*). This behavior was confirmed by estimating the exciton binding energies as a function of $n$ (figs. S3 and S4) (*17*), which amounts to 380 meV, 270 meV, and an average value of 220 meV for $n = 1$, $n = 2$, and $n > 2$, respectively. These values of exciton binding energy (>200 meV) attest to the robustness of the excitonic states at room temperature in phase-pure RPPs up to $n = 5$. They are about one order of magnitude larger than the values found in 3D lead halide perovskites (*19*) owing to quantum-confinement effects. Moreover, as compared to lead-salt (LS) materials in which dielectric-confinement effects become dominant, these values are similar to those of LS quantum dots (*20*), LS nanorods (*21*), and LS nanosheets (*22*) for similar confinement lengths (see detailed discussion in section ST1 of the supplementary materials and table S2) (*17*). For $n = 3$ to 5, the exciton binding energy reached a value of ~200 meV, consistent with a system exhibiting 2D quantum confinement, given negligible enhancement of the Coulomb interactions caused by dielectric confinement (*9*). However, in thin films the optical band gap is in good agreement with that observed for exfoliated crystals for $n = 1$ and 2 but red shifted by 200 to 300 meV for $n = 3$ to 5 (Fig. 1G).

We note that the band gap stayed almost constant in thin films with $n > 2$. Any modification to the pristine 2D perovskite phase during thin-film fabrication has already been excluded (*11, 12*). Effects such as changes in dielectric environment and differences in crystallinity (*23, 24*) cannot account for the redshifts observed in RPP thin films for $n > 2$. The redshifts are also not consistent with electronic impurities at surfaces, interfaces, or boundaries in perovskites where carriers are trapped a few tens of millielectron volts within the band gap (*25–28*). Furthermore, optical absorption anisotropy measurements (fig. S5) rule out effects from different orientations of the perovskite layers with respect to light polarization in both thin films and exfoliated crystals (*17*).

We further studied the microscopic origin of the low-energy band gap in thin films for $n > 2$ by confocal spatial mapping (~1-μm resolution)

[1]Los Alamos National Laboratory, Los Alamos, NM 87545, USA. [2]Department of Materials Science and Nanoengineering, Rice University, Houston, TX 77005, USA. [3]Department of Chemistry, Northwestern University, Evanston, IL 60208, USA. [4]Fonctions Optiques pour les Technologies de l'Information (FOTON), Institut National des Sciences Appliquées (INSA) de Rennes, CNRS, UMR 6082, 35708 Rennes, France. [5]Institut des Sciences Chimiques de Rennes (ISCR), Université de Rennes 1, CNRS, UMR 6226, 35042 Rennes, France. [6]Center for Functional Nanomaterials, Brookhaven National Laboratory, Upton, NY 11973, USA. [7]Department of Materials Science and Engineering, Northwestern University, Evanston, IL 60208, USA.
*Corresponding author. Email: jcrochet@lanl.gov (J.J.C.); amohite@lanl.gov (A.D.M.)

of the PL on a representative $n$ = 3 exfoliated crystal (Fig. 2A). Although the majority of the basal plane of exfoliated crystal yields spatially homogeneous PL at its band-gap energy (2.010 eV), appreciable PL emission was observed from the edges of the exfoliated crystal at 1.680 eV. Figure 2B illustrates the PL spectra of the exfoliated crystal, edges of the exfoliated crystal, and corresponding thin film. The spectra collected at the crystal edges contain PL peaks observed in both the thin film and exfoliated crystal, which indicates a common origin of the PL from states associated with the edges of the exfoliated crystal [labeled as layer-edge states (LESs)] and the PL at low energy in thin films for $n > 2$. Similar results were obtained in the case of $n$ = 4 and 5 RPP exfoliated crystals (fig. S6) (17), whereas the LES emission was absent when $n$ = 1 or 2.

We probed the spectral origin of the emitting states observed above using PL excitation (PLE) spectroscopy and time-resolved PL (TRPL). The PLE measurements were performed near the edges of the exfoliated crystal in Fig. 2A and revealed both the main exciton emission (labeled X state) at 2.010 eV and the LES at 1.680 eV. We monitored the PL intensity at the LES energy while sweeping the light-excitation energy between 1.800 and 2.900 eV (Fig. 2C). The PLE showed a clear peak at the position of the exciton (2.010 ± 0.007 eV) but no direct absorption into the LES was observed in the exfoliated crystal (PLE was negligible below 1.900 eV). The spectrum exhibited two high-energy features at ~2.110 and 2.200 eV, associated with excited excitonic states and band-to-band absorption, which yielded an exciton binding energy of 200 meV, in agreement with our absorption measurements (Fig. 1E).

These results and the comparable PL intensity of both the X state and LES features suggested that part of the photoexcited exciton population decayed to the LESs. This mechanism was further validated by probing the TRPL response of both states (Fig. 2D). At short times after the arrival of the light-excitation pulse, the exciton state became populated over a period of ~100 fs (25, 29) (not resolved here). However, the LES emission reached its maximum PL intensity ~200 ps after the X state, which is indicative of slow carrier filling from the higher-energy exciton to the low-energy edge states. We also observed a nearly fourfold increase in the carrier lifetime of the LES as compared with that of the exciton, suggesting suppressed nonradiative recombination of the localized carriers. Figure 2E schematically summarizes the photoemission mechanisms in 2D perovskites. The photoexcited exciton diffuses in the perovskite layer, emitting a photon at the exciton energy (geminate radiative recombination), or can be quenched through nonradiative recombination. However, these measurements elucidate that, in 2D perovskites with $n > 2$, a part of the photogenerated exciton population travels to the edges of the crystal within its diffusion time and then undergoes an internal conversion to a LES and efficiently emits photons at a lower energy than the main exciton.

We gained further insight into the physical origin of the optical transitions (Fig. 1, C and D) by analyzing the absorption and photoemission properties of thin films. Figure 3A describes the transitions in thin films with $n$ = 3 (see fig. S7 for the other $n$ values) (17). The absorption spectrum exhibits resonances at 1.947 ± 0.005, 2.067 ± 0.006, and 2.173 ± 0.006 eV, which are very close in energy to the main exciton state in exfoliated crystals (2.039 eV). These features were also observed in the PL spectra at relatively high light-excitation intensity $I_0$ (Fig. 3A, inset), i.e., after saturating the lower-energy LES population. The excitonic nature of these optical resonances was confirmed through (i) linear dependence of the integrated PL signal with respect to $I_0$ (Fig. 3B, black) and (ii) the negative temperature dependence of their peak energy (figs. S8 and S9) (5, 6, 17). On the other hand, the main PL peak at 1.695 ± 0.015 eV (Fig. 3A, inset) corresponds to the LES peak observed in exfoliated crystals (Fig. 2B). In sharp contrast to exfoliated crystals (Fig. 2), the PL was dominated by the LES peak, and a broad absorption feature around 1.73 eV (Fig. 3A) accounts for direct absorption into this LES and related minibands. These features are a direct consequence of both the light sampling across numerous LESs in thin films (Fig. 3D) because of preferential orientation of perovskite layers normal to the substrate (fig. S10) (12, 17), small grain sizes typically of the order of 200 to 400 nm (fig. S11) (12, 17), and the relaxation of optical-transition selection rules in imperfect crystals.

We also observed that the PL signal associated with the LES varied nonlinearly with the light-excitation intensity between $I_0^{1.30}$ and $I_0^{1.45}$ (Fig. 3B and fig. S7) (17). This signal corresponds to a mixed bimolecular and monomolecular recombination of photoexcited carriers (27), thus implying a partial dissociation of excitons to free carrier–like entities as the excitonic states convert (or dissociate) to the LESs. This conclusion is also consistent with the smooth rise of
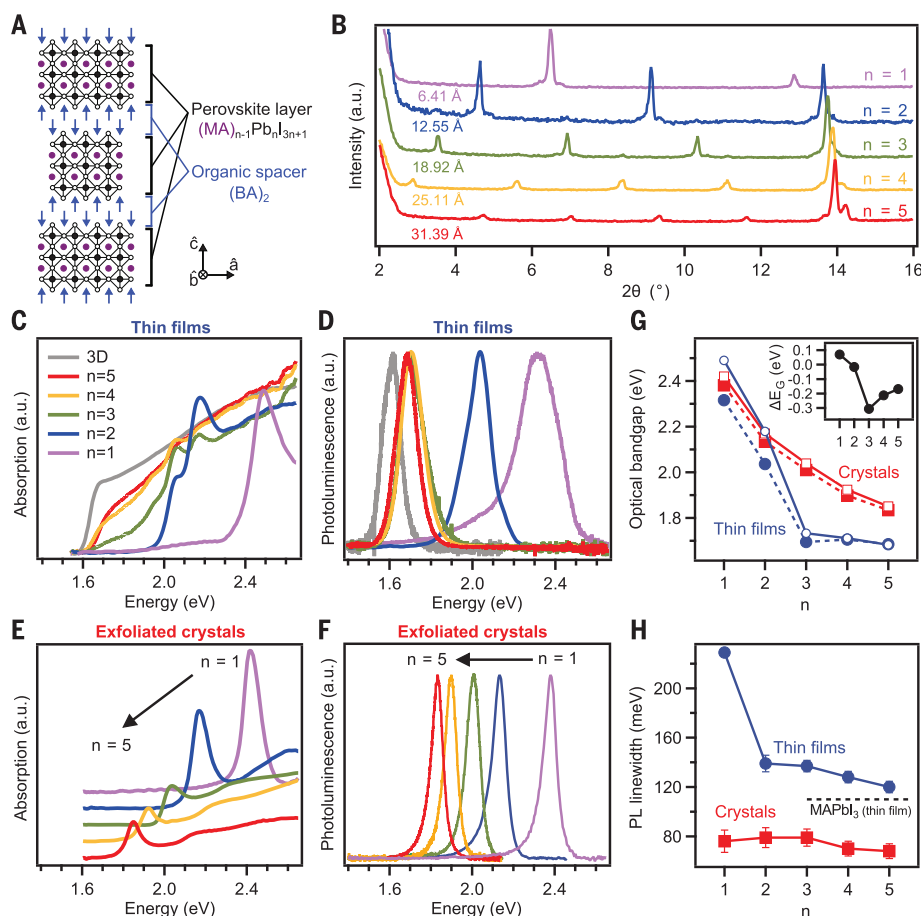


**Fig. 1. Evidence of phase purity of the RPPs ($n$ = 1 to 5) and comparison of optical properties of thin films and exfoliated crystals.** (**A**) Schematics of the QW-like crystal structure showing perovskite layers in the plane ($\hat{a}, \hat{b}$) sandwiched between organic spacing layers. (**B**) Phase purity established by monitoring the position and number of the low-angle peaks in x-ray diffraction patterns for each $n$ value. a.u., arbitrary units. Absorption and PL of the thin films (**C** and **D**) and exfoliated crystals (**E** and **F**). (**G**) Optical band gap derived from absorption (open symbols) and PL (filled symbols) as a function of $n$. (Inset) Shift of the optical band gap in thin films with respect to exfoliated crystals (from absorption). (**H**) PL linewidth versus $n$, showing inhomogeneous broadening in thin films as compared with that of exfoliated crystals.

the absorption at the optical band gap in comparison to the sharp excitonic features observed in exfoliated crystals (Fig. 1, C and E). Moreover, the energy of the LESs varied with temperature as 0.21 meV/K (fig. S12) (*17*), which has been attributed in 3D perovskites to the thermal expansion of the lattice where free carriers dominate (*30*). On the contrary, the RPPs with $n \leq 2$ that do not exhibit the LES showed negligible or negative temperature dependence of their optical resonances (fig. S8) (*17*), consistent with classical excitonic theory (*5, 6*).

All of these measurements establish a different physical origin and behavior of the excitonic and LES features and validate that the main band-gap optical transition in RPP thin films with $n > 2$ originates from the intrinsic electronic structure associated with the edges of the 2D perovskite layers (see discussion in section ST2 in the supplementary materials on the possible causes of LES formation) (*17*). Based on our observations, the primary mechanism that emerges in thin films is trapping of the free carriers after exciton dissociation to a deep electronic state located at layer edges. This model is compatible with both the higher PL efficiency and the longer lifetime of the LESs as compared with those of the higher-energy X states (Fig. 3, B and C). These results imply that, once the carriers are localized at LESs, they are protected from nonradiative decay mechanisms such as electron-phonon coupling (*31, 32*) or electronic impurities (*25*). These key mechanisms of the photoemission in RPPs are captured in Fig. 3E (fig. S13), where, after photogeneration of excitons (left), they can either decay through classical processes (dominant for $n \leq 2$, middle) or dissociate to free carriers potentially trapped at the LESs (dominant for $n > 2$, right). The process involving intrinsic dissociation of the primary photogenerated excitons to free carrier–like states that exist lower in energy in a single-component material is nonintuitive and not observed in any classical quantum-confined material system.

Motivated by the observed internal exciton dissociation from a part of the higher-energy excitonic states to the LESs that protect the carriers
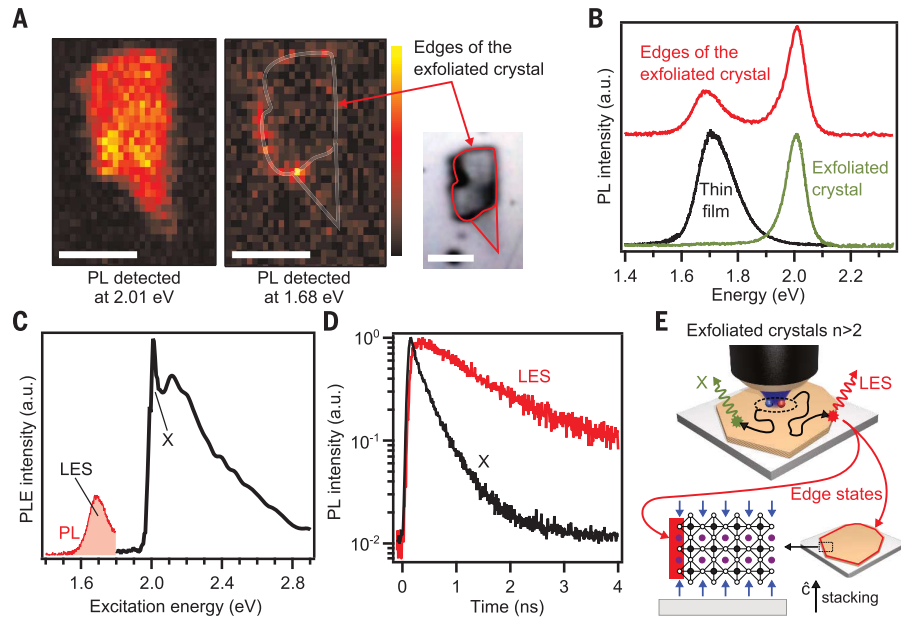


**Fig. 2. Microscopic origin of the low-energy band gap in 2D perovskite thin films for $n = 3$. (A)** PL-intensity map of a single exfoliated crystal, probed at 2.010 and 1.680 eV. (Right) Microscopy image showing the layer edges of the exfoliated crystal. Scale bar, 10 μm. **(B)** Comparison of the PL in the exfoliated crystal, at the exfoliated-crystal edges, and in the corresponding thin film. **(C)** PLE-integrated signal of the LES, measured by locally exciting the exfoliated-crystal edges. The measured PL profile of the LES is also plotted. **(D)** TRPL of the PL features X state and LES observed in (B) and (C). **(E)** Schematics of the photoabsorption and PL processes in 2D perovskite exfoliated crystals with $n > 2$.



**Fig. 3. Optical absorption and emission mechanisms in thin films of 2D perovskites. (A)** Thin film $n = 3$ absorption (green), PL at photoexcitation 100 mW/cm$^2$ (black) and 10$^6$ mW/cm$^2$ (red). **(B)** $I_0$ dependence of the integrated PL. Dashed lines are fits to the data. **(C)** TRPL in the thin films $n = 3$. (Inset) Corresponding lifetimes ($\tau$) of the X states and LESs as a function of the $n$ value. Excitation at ~100 mW/cm$^2$. **(D)** Schematics of the photoabsorption and PL processes in a 2D perovskite thin film with $n > 2$. In contrast to exfoliated crystals, thin-film perovskite layers are preferentially oriented normal to the substrate (fig. S10) (*12, 17*), therefore, excitation light probes numerous amounts of LESs. **(E)** Summary of the main photoemission mechanisms in thin films. The diffusion length was estimated from fig. S13 (*17*). VB and CB stand for valence and conduction bands, respectively.
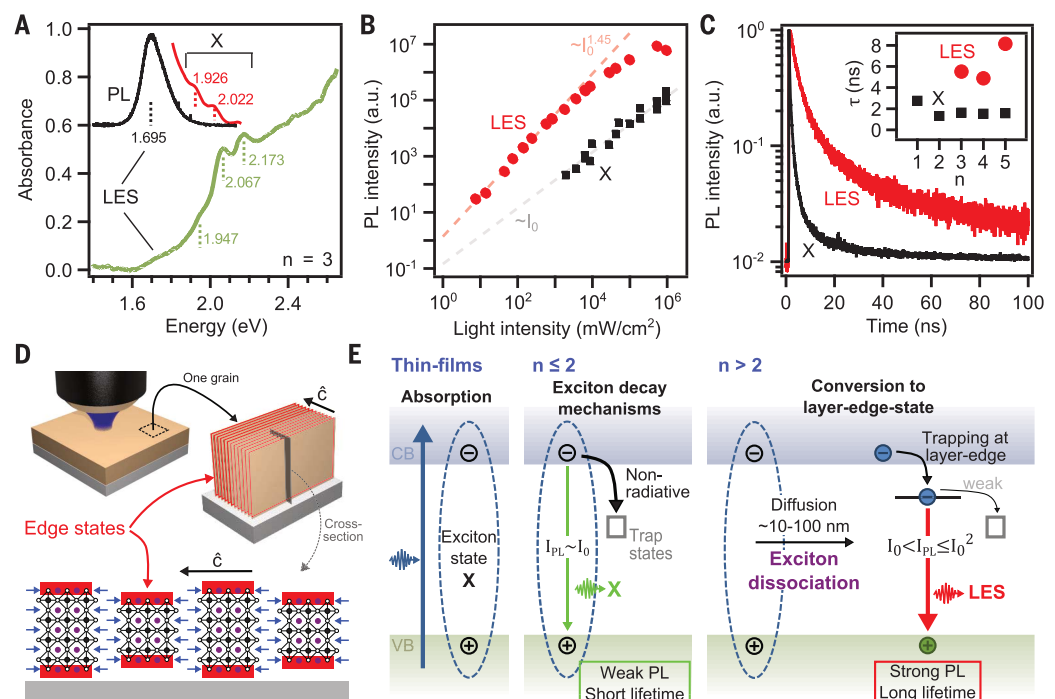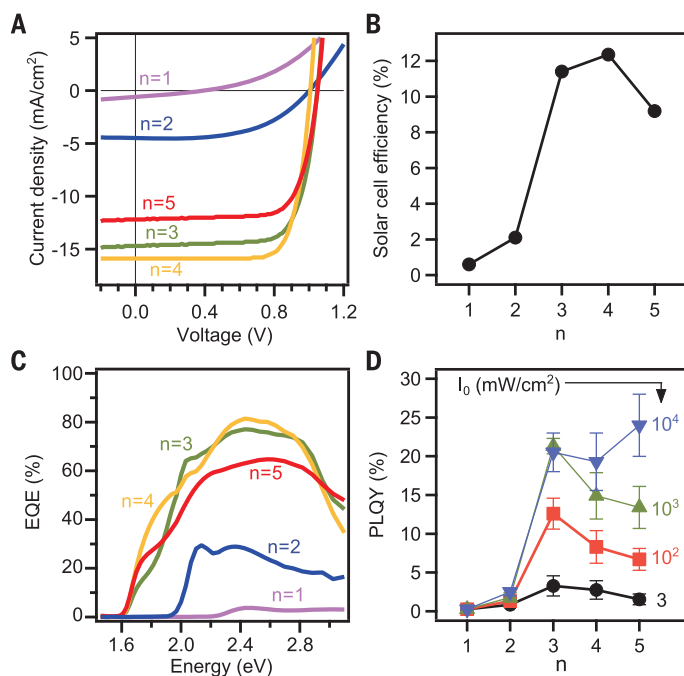
**Fig. 4. Figures of merit of thin-film devices for light-harvesting and solid-state emission.** (**A**) *J-V* characteristics measured under AM1.5 illumination. (**B**) Power-conversion efficiency as a function of 2D perovskite *n* value (QW thickness). (**C**) EQE for the PV devices in (A). (**D**) PLQY in thin films as a function of *n* value for several light-excitation intensities.



over an appreciably longer time scale, we fabricated high-efficiency PV cells with RPPs and measured their current-voltage (*J-V*) characteristics and power conversion efficiency (PCE) (Fig. 4, A and B). We observed a sharp break in the current density and PCE from <2% for *n* = 1 and 2 to >12% for *n* > 2. Assuming comparable charge-transport properties for all RPPs, the performances of PV cells for *n* > 2 are impacted by the presence of the LES as (i) it extends the absorption from the visible to the near infrared and (ii) it contributes to internal exciton dissociation to free carrier–like entities that can be more readily collected by the built-in field in a PV device. This was confirmed by measuring the external quantum efficiency (EQE) spectra (Fig. 4C), which showed about fivefold enhancement in collection efficiency in PV cells using RPPs with *n* > 2 as compared to RPPs with *n* = 1 and 2. Furthermore, the free carriers that converge to the LESs remain protected, thus exhibiting long recombination carrier lifetimes resulting in a much higher probability for efficient PL (Fig. 4D and fig. S14) (*17*), which has tremendous implications for high-efficiency light-emitting devices using RPPs with *n* > 2. The variations of the PL efficiency in thin films and of the solar cell efficiency (*33*) between RPPs with *n* = 3, 4, and 5 were possibly due to small variations of

the crystal crystallinity and ordering (*12*) and/or light out-coupling and photon-recycling effects (*34*). These results not only pave the path forward for the rational design of high-efficiency optoelectronic devices with solution-processed layered 2D perovskite-based materials, but they are also relevant to a large group of materials with edges and surface states.

## REFERENCES AND NOTES

1. S. N. Ruddlesden, P. Popper, *Acta Crystallogr.* **10**, 538–539 (1957).
2. S. N. Ruddlesden, P. Popper, *Acta Crystallogr.* **11**, 54–55 (1958).
3. C. R. Kagan, D. B. Mitzi, C. D. Dimitrakopoulos, *Science* **286**, 945–947 (1999).
4. C. C. Stoumpos *et al.*, *Chem. Mater.* **28**, 2852–2867 (2016).
5. T. Ishihara, J. Takahashi, T. Goto, *Phys. Rev. B Condens. Matter* **42**, 11099–11107 (1990).
6. N. Kitazawa, M. Aono, Y. Watanabe, *J. Phys. Chem. Solids* **72**, 1467–1471 (2011).
7. J. Even, L. Pedesseau, C. Katan, *ChemPhysChem* **15**, 3733–3741 (2014).
8. D. Sapori, M. Kepenekian, L. Pedesseau, C. Katan, J. Even, *Nanoscale* **8**, 6369–6378 (2016).
9. L. Pedesseau *et al.*, *ACS Nano* **10**, 9776–9786 (2016).
10. I. C. Smith, E. T. Hoke, D. Solis-Ibarra, M. D. McGehee, H. I. Karunadasa, *Angew. Chem. Int. Ed.* **53**, 11232–11235 (2014).
11. D. H. Cao, C. C. Stoumpos, O. K. Farha, J. T. Hupp, M. G. Kanatzidis, *J. Am. Chem. Soc.* **137**, 7843–7850 (2015).
12. H. Tsai *et al.*, *Nature* **536**, 312–316 (2016).
13. K. Tanaka, T. Kondo, *Sci. Technol. Adv. Mater.* **4**, 599–604 (2003).
14. K. Tanaka *et al.*, *Jpn. J. Appl. Phys.* **44**, 5923–5932 (2005).
15. K. Gauthron *et al.*, *Opt. Express* **18**, 5912–5919 (2010).
16. D. B. Mitzi, K. Chondroudis, C. R. Kagan, *IBM J. Res. Develop.* **45**, 29–45 (2001).
17. Materials and methods are available as supplementary materials.
18. O. Yaffe *et al.*, *Phys. Rev. B* **92**, 045414 (2015).
19. L. M. Herz, *Annu. Rev. Phys. Chem.* **67**, 65–89 (2016).
20. J. Jasieniak, M. Califano, S. E. Watkins, *ACS Nano* **5**, 5888–5902 (2011).
21. A. C. Bartnik, A. L. Efros, W.-K. Koh, C. B. Murray, F. W. Wise, *Phys. Rev. B* **82**, 195313 (2010).
22. J. Yang, F. W. Wise, *J. Phys. Chem. C* **119**, 26809–26816 (2015).
23. J.-C. Blancon *et al.*, *Nat. Commun.* **4**, 2542 (2013).
24. Y. Lin *et al.*, *Nano Lett.* **14**, 5569–5576 (2014).
25. X. Wu *et al.*, *J. Am. Chem. Soc.* **137**, 2089–2096 (2015).
26. W. Nie *et al.*, *Science* **347**, 522–525 (2015).
27. J.-C. Blancon *et al.*, *Adv. Funct. Mater.* **26**, 4283–4292 (2016).
28. D. W. de Quilettes *et al.*, *Science* **348**, 683–686 (2015).
29. K. Abdel-Baki *et al.*, *J. Appl. Phys.* **119**, 064301 (2016).
30. H. Wang, L. Whittaker-Brooks, G. R. Fleming, *J. Phys. Chem. C* **119**, 19590–19595 (2015).
31. Z. Guo, X. Wu, T. Zhu, X. Zhu, L. Huang, *ACS Nano* **10**, 9992–9998 (2016).
32. D. B. Straus *et al.*, *J. Am. Chem. Soc.* **138**, 13798–13801 (2016).
33. O. D. Miller, E. Yablonovitch, S. R. Kurtz, *IEEE J. Photovolt.* **2**, 303–311 (2012).
34. J. M. Richter *et al.*, *Nat. Commun.* **7**, 13941 (2016).

## SUPPLEMENTARY MATERIALS

www.sciencemag.org/content/355/6331/1288/suppl/DC1
Materials and Methods
Supplementary Text
Figs. S1 to S14
Tables S1 and S2
References (*35–40*)

Editor's Summary

### How perovskites have the edge

Two-dimensional Ruddlesden-Popper perovskites form quantum wells by sandwiching inorganic-organic perovskite layers used in photovoltaic devices between organic layers. Blancon *et al.* show that if the perovskite layer is more than two unit cells thick, photogenerated excitons undergo an unusual but highly efficient process for creating free carriers that can be harvested in photovoltaic devices (see the Perspective by Bakr and Mohammed). Lower-energy local states at the edges of the perovskite layer facilitate dissociation into electrons and holes that are well protected from recombination.

*Science*, this issue p.1288; see also p. 1260

| | |
|---|---|
| **Article Tools** | Visit the online version of this article to access the personalization and article tools:<br>http://science.sciencemag.org/content/355/6331/1288 |
| **Permissions** | Obtain information about reproducing this article:<br>http://www.sciencemag.org/about/permissions.dtl |